Catalysis Letters
https://doi.org/10.1007/s10562-019-02933-1

Chirally-Modified Graphite Oxide as Chirality Inducing Support for Asymmetric Epoxidation of Olefins with Grafted Manganese Porphyrin

Elahe Ahadi[1] · Hassan Hosseini-Monfared[1,2] · Carsten Schlüsener[3] · Christoph Janiak[3] · Afsaneh Farokhi[1]

Received: 15 March 2019 / Accepted: 31 August 2019

Abstract

A chirality inducer was prepared by graphite oxide (GO) functionalization with enantiopure L-tartrate (GO*) and used as asymmetric support for a covalently-linked manganese porphyrine complex [Mn(TPyP)OAc]. The thereby obtained heterogeneous catalyst, GO*-[Mn(TPyP)OAc], showed excellent performance and ee-values of 92–99% for the asymmetric epoxidation of prochiral olefins with O_2 as oxidant and isobutyraldehyde as co-reductant in acetonitrile; linear terminal olefins with 54–76% conversion and quantitative conversion of aromatic olefins. The GO*-[Mn(TPyP)OAc] catalyst is highly active, recyclable, and at the same time simple and inexpensive to prepare with a chiral inducer from the chiral pool. The structure of the catalyst was elucidated by scanning electron microscopy (SEM), transmission electron microscopy (TEM), BET analysis, FT-IR, Raman, and photoluminescence spectroscopic methods.

Graphic Abstract

Graphite oxide functionalized with an enantiopure group was used as a chirality inducer and asymmetric support for a Mn-porphyrine complex. The thereby obtained heterogeneous catalyst is an excellent enantioselective catalyst for the epoxidation of prochiral olefins.

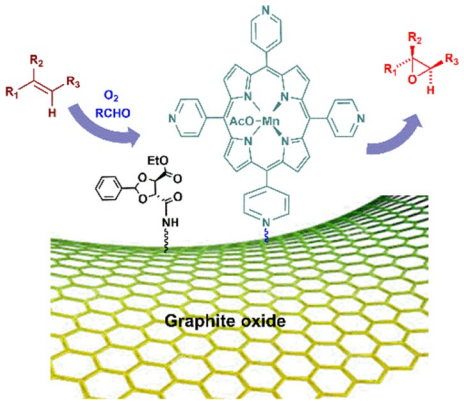

Keywords Chiral epoxidation · Oxygen · Manganese porphyrin · Graphite oxide · Heterogeneous catalysis

1 Introduction

Most biologically important molecules are chiral. Therefore, preparation of enantiomerically pure chemicals is an important topic in many areas of society and science, and as a result there is a lot of interest on the topic of preparation of

Electronic supplementary material The online version of this article (https://doi.org/10.1007/s10562-019-02933-1) contains supplementary material, which is available to authorized users.

✉ Hassan Hosseini-Monfared
hahomonfared@gmail.com

Extended author information available on the last page of the article

Published online: 13 September 2019

chiral materials [1–4]. The epoxidation reaction is an attractive C–O bond forming reaction in which an olefin compound is oxidized to an epoxide, which may be subsequently transformed to a variety of functional groups, such as alcohol, carbonyl, diol, azide, etc. In many of these transformations, the stereogenic centers formed in the addition reaction are kept, so enantioselective versions of this reaction were developed on the basis of the use of chiral catalysts. Asymmetric catalysis is the best method from the atom-economic point of view to selectively produce single enantiomers in the pharmaceutical and agrochemical industry [5, 6]. For separation and reuse of the relatively expensive catalysts from the reaction mixture at the end of the process, heterogenization of chiral catalysts is essential [7, 8]. Heterogenization of molecular catalysts sometimes improves their selectivity compared to the homogeneous ones through site-isolation, constraint and synergistic effects [9–11]. However, the use of heterogenized catalysts has usually serious limitations such as low reactivity, cost and the tedious procedure involved in designing the catalysts [12]. Therefore, there is a continuing need to develop more efficient and practical heterogenization methods for chiral catalysts.

For a heterogeneous chiral catalyst, a very successful strategy to induce chirality relied on the use of chiral ligands immobilized onto the support material [13]. Various methods of noncovalent immobilization techniques such as entrapment, ion exchange or adsorption have been used to prevent the loss of the optimal geometry of the catalyst or chemical change of the chiral ligand [13, 14], however, they were not completely successful. Alternatively, in an interesting study, cellulose nanocrystals were used as enantioselective support for the immobilization of Pd patches in the hydrogenation of prochiral ketones with high enantiomeric excess in water at 4 bar H_2 [15]. In another study, the mixed-ligand strategy, the usage of a chiral *N*-carbamylglutamate and an achiral bispyridine ligand, was applied to prepare homochiral neutral layered coordination polymers [16]. Adsorption of chiral modifiers onto non-chiral metal surfaces was also investigated to create effective heterogeneous catalysts [17, 18]. Gellman and coworkers have summarized the latest report on chiral surface chemistry which was performed on model single crystalline surfaces [19]. It has been suggested that the energetic differences in the interaction of prochiral substrates with a chiral surface results in enantioselectivity for the products.

Graphene is a single-layer sheet from graphite, consisting of carbon atoms with sp^2 hybridization and honeycomb configuration. It possesses a high thermal conductivity and a high surface area of 2630 $m^2\ g^{-1}$ [20] that makes it a superior candidate, in comparison to SBA-15, MCM-41 and conventional MOFs, to be used as a support for the heterogenization of catalysts. Oxygen-containing functional groups of graphite oxide (GO) help to anchor metal–organic ligand complexes to GO. Furthermore, the synergic interactions between the complex and GO can improve the complex activity [21]. Additionally, the required large specific surface area of the resulting hybrid materials for catalysis is obtained by exfoliation of GO sheets during the complex-grafting reaction, with the anchored complexes then preventing a new aggregation [22]. Based on the above-mentioned studies, we have set out to prepare a chiral graphite oxide (GO^*) as chirality-inducing support for the asymmetric epoxidation of olefins with grafted manganese porphyrin and molecular oxygen. In comparison with other oxidants such as $NaIO_4$/imidazole, NaClO/4-phenylpyridine *N*-oxide (PPNO) and m-CPBA/*N*-methylmorpholine *N*-oxide (NMO), molecular oxygen is an ideal oxidant in the epoxidation of olefins to the corresponding epoxides catalyzed by metalloporphyrins because of its low cost and environmentally friendly nature [23].

2 Experimental Section

2.1 Materials

5,10,15,20-Tetra(4-pyridyl)porphyrin (H_2TPyP) (95%) was obtained from Fluka, (2*R*,3*R*)-(+)-tartaric acid, (L-(+)-tartaric acid, 99%) from Merck. The other reagents and chemicals used for experiments were purchased from Merck with highest purity. Deionized water was used for all experiments.

For analysis of the reaction products an HP Agilent 6890 gas chromatograph equipped with an HP-5 capillary column (phenyl methyl siloxane 30 m × 320 μm × 0.25 μm) with flame-ionization detector was used. The enantiomeric excess (ee) was determined by an HP 6890-GC using a chiral SGE-CYDEX-B capillary column (25 m × 0.22 mm ID × 0.25 μm). ^{1}H-NMR spectra were recorded on a Bruker 250 MHz spectrometer using $CDCl_3$ as solvent, with the residual proton solvent peak as reference and calibrated against TMS.

UV–Vis spectra of the solutions were run on a Shimadzu 160 spectrometer. Fourier transform infrared (FT-IR) spectra were taken using a Perkin-Elmer 597 spectrophotometer. Powder X-ray diffraction patterns were collected at a Bruker D8 ADVANCE, wavelength 1.5406 Å (Cu Kα), voltage 40 kV, current 40 mA. Scanning electron microscope (SEM) were acquired using a Hitachi F4160 SEM operated at an accelerating voltage of 10 kV or a JEOL JSM-6510 Advanced electron microscope (Jeol, Akishima, Japan) with a LaB_6 cathode at 5–20 keV. The microscope was equipped with an Xflash 410 (Bruker) silicon drift detector for energy-dispersive X-ray spectroscopic (EDX) elemental analysis. TEM images were recorded with a Zeiss 902A electron microscope. The samples were prepared by suspending the samples in acetonitrile under short ultrasonication and

dripping the suspension onto a carbon-coated copper grid and letting it dry. BET method was employed to perform the specific surface area analysis, using a Micromeritics ASAP 2020 analyzer. Alternatively, nitrogen (purity 99.9990%) physisorption isotherms were carried out on an Autosorb-6 from Quantachrome at 77 K. The manganese content of the catalyst was measured by a Varian spectrometer AAS-110.

2.2 Graphite Oxide Synthesis

Graphite powder was oxidized using the improved synthesis method of graphite oxide by Marcano et al. [24]. Typically, to a mixture of graphite powder (0.5 g) and $KMnO_4$ (3.0 g), the mixture of concentrated H_2SO_4/H_3PO_4 (60:6 mL) was added dropwise under ice-cooling. The resulting suspension was stirred for 30 min in an ice bath, then it was heated at 70 °C for 24 h. After cooling to RT 1.5 mL of 35% H_2O_2 in ice was added to remove the unreacted $KMnO_4$ reagent. Finally, the obtained yellow solid was washed consecutively with deionized water (30 mL), 30% HCl solution (30 mL), EtOH (200 mL) and diethyl ether (30 mL). Yield: 0.40 g.

2.3 Synthesis of Amine-Functionalized Graphite Oxide, GO(NH_2)

Following the reported procedure by Bhanja et al. the hydroxyl and carboxyl groups of the GO surfaces were used for grafting 3-aminopropyl groups [25]. First GO (0.66 g) was sonicated in dry toluene (46 mL) for 20 min, then a solution of 3-aminopropyltriethoxysilane (2 mL) in dry toluene (13 mL) was added slowly into the GO/toluene suspension and the combined mixture was refluxed under nitrogen atmosphere for 24 h. The resulting amine-functionalized product, GO(NH_2), was filtered and washed thoroughly with dry toluene (3 × 2 mL) to remove unreacted 3-aminopropyltrimethoxysilane. The dark black solid was dried at 70 °C for 6 h. Yield: 0. 56 g. CHN analysis of GO(NH_2): C 36.83%, H 4.69%, N 6.26%, molar C/N ratio = 6.82.

2.4 Synthesis of GO-tart (GO*)

The mixture of diethyl-2,3-*O*-benzylidene-L-tartrate (12 mg, 0.041 mmol) and amine-functionalized graphene (GO(NH_2), 0.18 g) in methanol (5 mL) was refluxed for 2 h and the resulting product was washed with water (10 mL) and dried in air. Yield: 0.17 g. CHN analysis of GO-tart: C 38.96%, H 4.73%, N 6.18%, molar C/N ratio = 7.00.

2.5 Functionalization of GO(NH_2) by Chloropropyl, GO(NH_2)(Cl)

GO(NH_2) (0.16 g) was sonicated in dry toluene (13 mL) for 20 min. After addition of a solution of 3-chloropropyltrimethoxysilane (0.86 mL) in 3.5 mL of dry toluene, the mixture was refluxed for 24 h under nitrogen atmosphere. The black powdery sample was separated by filtration after cooling to room temperature and washed several times with toluene (3 × 2 mL) and EtOH (3 × 2 mL). The resulting product GO(NH_2)(Cl) was dried at 70 °C for 6 h. Yield: 0. 14 g.

2.6 Synthesis of [Mn(TPyP)OAc]

For the metalation of H_2TPyP, 0.80 g (1.29 mmol) of H_2TPyP and 3.16 g (12.9 mmol, 10 equiv.) of $Mn(OAc)_2{\cdot}4H_2O$ were dissolved at room temperature in 100 mL of glacial acetic acid and heated at 80 °C for 6 h. From the resulting solution the solvent was removed in a rotary evaporator and the solid residue dissolved in 1000 mL of water at 60 °C. The solution was filtered and the metalloporphyrin was precipitated by the addition of 100 mL of sodium acetate solution (2 mol/L). Yield: 0.76 g, 81%.

2.7 Immobilization of [Mn(TPyP)OAc] on GO(NH_2)(Cl)

The amino- and chloro-functionalized graphite oxide GO(NH_2)(Cl) (0.15 g) and [Mn(TPyP)OAc] (15 mg, 0.0205 mmol) were dispersed in DMF (30 mL) and the suspension was heated at 100 °C for 48 h under vigorous stirring. The obtained black precipitate was washed with methanol and ether. The resulting GO(NH_2)-[Mn(TPyP)OAc]$^+Cl^-$ was dried at 60 °C for 6 h. Yield: 99 mg.

2.8 Functionalization GO(NH_2)-[Mn(TPyP)OAc]$^+Cl^-$ by Tartrate Ester

Diethyl-2,3-*O*-benzylidene-L-tartrate was synthesized following a procedure developed by our group [26]. The dispersion of diethyl-2,3-*O*-benzylidene-L-tartrate (1.7 mg, 0.0058 mmol) and GO(NH_2)-[Mn(TPyP)OAc]$^+Cl^-$ (26.4 mg) in methanol (10 mL) was refluxed for 72 h. After cooling to room temperature, the resulting product GO*-[Mn(TPyP)OAc]$^+Cl^-$ was washed with water (10 mL) and dried in air [27]. Atomic absorption measurement showed 26 µmol Mn or 1.4 mg Mn per gram of GO*-[Mn(TPyP)OAc]$^+Cl^-$, corresponding to 0.14 wt% Mn. This low Mn content was in agreement with its EDX analysis (see Supplementary Information).

2.9 Catalytic Oxidation of Styrene with Molecular Oxygen

Styrene was used as a representative prochiral olefin. The catalytic activity of GO*-[Mn(TPyP)OAc]$^+Cl^-$ was investigated for the oxidation of styrene in a 25 mL round bottom

flask equipped with a magnetic stirring bar and a reflux condenser at the determined temperature (20 °C, 40 °C and 60 °C). The olefin substrate (1 mmol), catalyst (1.0 mg) and isobutyraldehyde (3 mmol) were dispersed in 3 mL of solvent (*n*-hexane, acetonitrile, and ethyl acetate) and oxygen was provided by a balloon. The reaction was continued for a determined time (2 h, 4 h, 6 h). During the reaction, aliquots of the reaction mixture (2 µL) were withdrawn and analysed by GC. Authentic samples and spectroscopic methods were used for the identification of the products. For GC with HP-5 capillary column: injection temperature 250 °C, detector temperature 250 °C, carrier gas N_2 flow rate 0.70 mL/min; the oven temperature was held at 90 °C for 0.1 min, then heated to 190 °C at a rate of 10 °C min^{-1} and kept for 5 min. For chiral GC with SGE-CYDEX-B capillary column, a column flow of 0.70 mL min^{-1} was applied. The detector and injection temperatures were 200 °C. The oven temperature was held at 50 °C for 0.1 min, then the temperature was increased to 150 °C at a rate of 7 °C min^{-1} and kept for 15 min. Moreover, the reusability and time stability of catalyst GO*-[Mn(TPyP)OAc]$^+Cl^-$ were examined under the same reaction conditions as that of the first catalytic run.

For the manganese leaching test in the oxidation of styrene, the solid catalyst GO*-[Mn(TPyP)OAc]$^+Cl^-$ was removed from the reaction mixture after 6 h by centrifugation. The supernatant was decanted, 1 mL of concentrated H_2SO_4 added and the mixture was refluxed for 1 h. The resulting solution was investigated by UV–Vis absorption spectroscopy and atomic absorption spectrometry.

3 Results and Discussion

3.1 Synthesis of Catalyst

Graphite oxide is an attractive support material since it is thermally, chemically, and mechanically stable during the reaction process and has a large surface area as well. GO consists of oxygen-containing functional groups such as hydroxyl, carbonyl, and epoxy on the basal graphite plane [28], and it can be well-dispersed in polar solvents such as water. Furthermore, GO is known to be a good substrate for the dispersion of catalytically active nanoparticles [29] and for the stabilization of the immobilized metal-complexes [20, 30–32]. The chiral heterogeneous catalyst GO*-[Mn(TPyP)OAc]$^+Cl^-$ was synthesized as follows. First, the prepared GO was functionalized with aminopropyl and chloropropyl to produce GO(NH_2)(Cl), Scheme 1a. Second, the manganese–tetrapyridylporphyrin complex was covalently attached to GO(NH_2)(Cl) through quaternization of the pyridyl nitrogen atom of [Mn(TPyP)OAc] by reaction with the formation of a pyridinium chloride moiety with a covalent link between the carbon atom of the former chloropropyl unit and the pyridyl nitrogen atom in the compound GO(NH_2)-[Mn(TPyP)OAc]$^+Cl^-$, Scheme 1b. Finally, functionalization of GO through the aminopropyl groups by a chiral, enantiopure L-tartrate derivative led to chiral GO*-[Mn(TPyP)OAc]$^+Cl^-$, Scheme 1c. For the synthesis of the chiral tartrate unit, (2*R*,3*R*)-tartaric acid was treated with ethanol to produce the corresponding ester and then its dihydroxyl groups were protected by benzaldehyde in the presence of *p*-toluenesulfonic acid [26].

The specific surface areas were calculated according to the Brunauer–Emmett–Teller (BET) method from N_2 adsorption isotherms at 77 K for GO(NH_2)-[Mn(TPyP)OAc]$^+Cl^-$ and GO*-[Mn(TPyP)OAc]$^+Cl^-$ to 50 m^2/g and 44 m^2/g, respectively. The two surface areas are within experimental error to each other. In comparison to GO, the development of a porous structure contributed to the increase in the BET surface area of GO(NH_2)-[Mn(TPyP)OAc]$^+Cl^-$ and GO*-[Mn(TPyP)OAc]$^+Cl^-$, and this has been confirmed by N_2 adsorption–desorption analysis (Table 1). The pore volume of GO(NH_2)-[Mn(TPyP)OAc]$^+Cl^-$ do not change after functionalization with enantiopure L-tartrate. The lower results observed for the GO sample could be attributed to the incomplete re-stacking of GO material layers and nearby blocked pores. GO is prone to re-stacking owing to active π–π interactions and van der Waals forces connecting the nearly planar planes of GO sheets [33].

3.2 FT-IR spectra

FT-IR analysis proved the presence of [Mn(TPyP)OAc]$^+Cl^-$ on the surface of the GO* sample. Upon functionalization of GO, significant changes were observed in the FT-IR data with respect to the GO spectrum which indicated an effective functionalization. Figure 1 compares the FT-IR spectra recorded on GO, GO(NH_2), GO(NH_2)(Cl), GO-[Mn(TPyP)OAc]$^+Cl^-$ and GO*-[Mn(TPyP)OAc]$^+Cl^-$ samples from 650 to 2000 cm^{-1}. Many of the spectral features in the fingerprint region between 700 and 1400 cm^{-1} decrease in intensity when going from neat GO to the functionalized GO samples. Vibrations in this fingerprint region mainly correspond to ν_{C-O-C} (~ 854 and 1227 cm^{-1}), δ_{OH} (~ 1379 cm^{-1}) and ν_{C-OH} (~ 1053 cm^{-1}), i.e. originating from the epoxy, alcohol and carbonyl groups from GO [34]. The elimination of these groups upon functionalization was confirmed by their disappearance in GO-derived samples. Additionally, the peaks at ~ 1820 cm^{-1} and 1735 cm^{-1} are seen only in the pristine GO sample. These peaks are related to $\nu_{C=O}$ from carbonyl groups [34]. The two different peaks can be related to isolated (absorbing at 1820 cm^{-1}) carbonyl groups and C=O which is H-bonded to nearby OH groups or water molecules (peak at 1735 cm^{-1}). The carboxylic groups also contribute at the peak 1735 cm^{-1}. While the peak at 1735 cm^{-1} appeared with decreased intensity in the sample

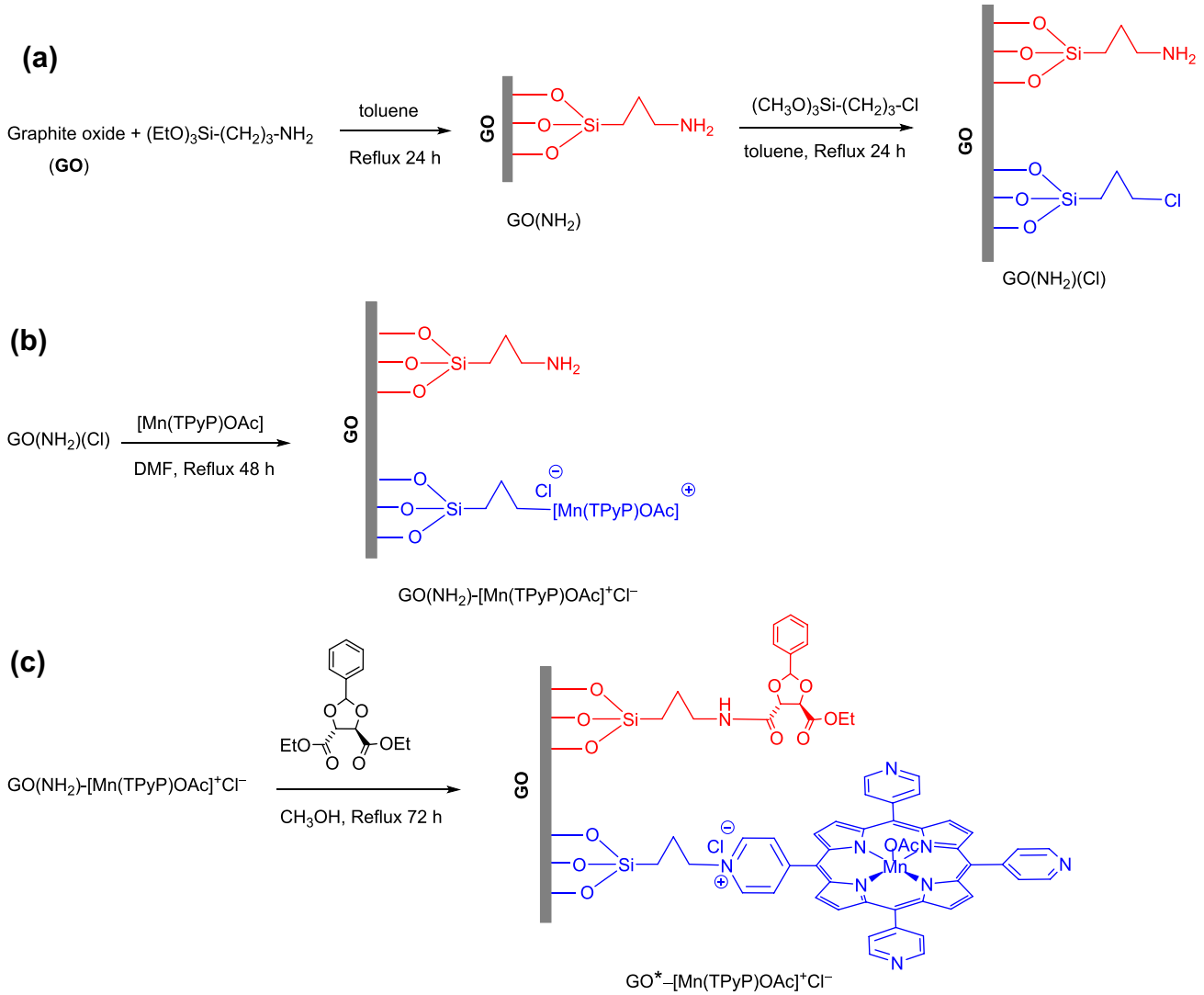

Scheme 1 Synthesis of chiral heterogeneous catalyst GO*-[Mn(TPyP)OAc]$^+$Cl$^-$

Table 1 Surface area and pore volume of GO, GO(NH$_2$)-[Mn(TPyP)OAc]$^+$Cl$^-$ and GO*-[Mn(TPyP)OAc]$^+$Cl$^-$

Sample	BET surface area ($m^2\ g^{-1}$)	Pore volume ($cm^3\ g^{-1}$)	Pore diameter (nm)
GO	3	0.010	7
GO(NH$_2$)-[Mn(TPyP)OAc]$^+$Cl$^-$	50	0.084	43
GO*-[Mn(TPyP)OAc]$^+$Cl$^-$	44	0.089	44

GO(NH$_2$), the peak at 1820 cm^{-1} completely disappeared on all functionalized samples. This confirms that most of the carbonyl groups are eliminated with GO silylation. The peak centered at ~ 1623 cm^{-1} is attributed to $\nu_{C-C(aromatic)}$ on GO [34]. Although the changes in the FT-IR spectrum of GO*-[Mn(TPyP)OAc]$^+$Cl$^-$ with respect to those of GO-[Mn(TPyP)OAc]$^+$Cl$^-$ and GO(NH$_2$)(Cl) are small, fluorescence studies (see the next section) confirmed the grafting of Mn-porphyrin onto GO*.

3.3 Photoluminescence Property

Porphyrins and GO show fluorescence because of having multiple conjugated double bonds with high degree of resonance stability. They have delocalized π-electrons that can be placed in low-lying excited singlet states [35]. The solid-state luminescent properties of GO*-[Mn(TPyP)OAc]$^+$Cl$^-$ together with free GO and GO* were investigated at room temperature. From Fig. 2, it can be seen that a broad emission band is centered at 483 nm for GO, GO* and GO*-[Mn(TPyP)OAc]$^+$Cl$^-$ (λ_{ex} = 405 nm). While GO

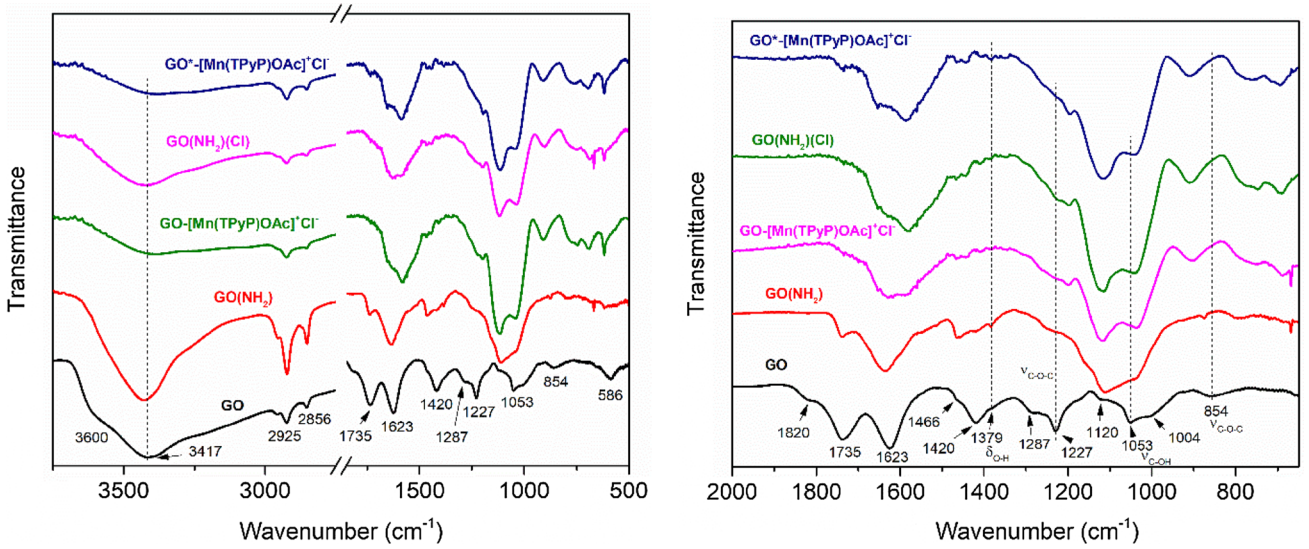

Fig. 1 FT-IR spectra of GO, $GO(NH_2)$, $GO(NH_2)(Cl)$, GO-$[Mn(TPyP)OAc]^+Cl^-$ and GO^*-$[Mn(TPyP)OAc]^+Cl^-$

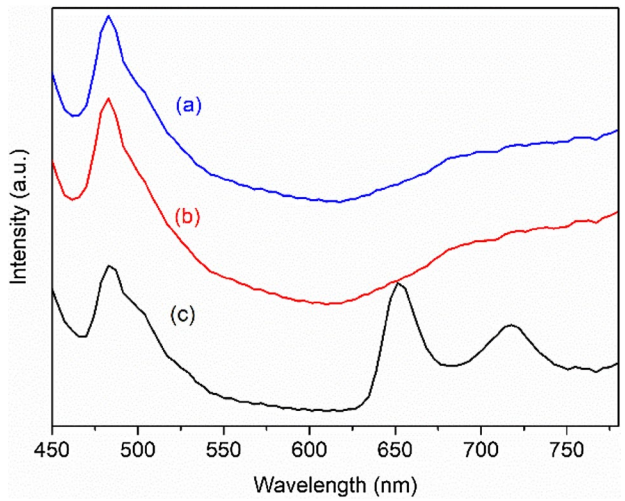

Fig. 2 Solid-state emission spectra (upon excitation at λ = 405 nm) of (a) GO, (b) GO^* (GO-tart) and (c) GO^*-$[Mn(TPyP)OAc]^+Cl^-$; 1.0 mg sample dispersed in 3 mL of *N*,*N*-dimethylformaide

and GO^* have similar emission spectra, GO^*-$[Mn(TPyP)OAc]^+Cl^-$ feature two additional emission bands at 652 and 718 nm. The observation above suggests that its luminescent mechanism possibly originates from the [Mn(TPyP)OAc]-centered emission. In addition, the fluorescence emission confirms the presence and immobilization of [Mn(TPyP)OAc] on GO^*. The fluorescence bands in the 600–800-nm range of the emission spectra of metalloporphyrins result from S1 → S0 transitions; the individual bands correspond to the (0,0), (0,1) and (0,2) transitions with respect to vibrational states [36].

3.4 Thermogravimetric Analysis

Typical thermogravimetric (TGA) curves of $GO(NH_2)$, GO-tart and GO^*-$[Mn(TPyP)OAc]^+Cl^-$ are shown in Fig. 3 to analyze the thermal stabilities through the temperature-dependent weight loss of the materials. Weight loss is observed for GO in several steps (Fig. S1 in Supplementary Information). The residual water is lost by heating to 100 °C. The second weight loss (39%) occurs at about 100 °C to 200 °C, probably due to the decomposition of the oxygen-containing functional groups of GO. The weight loss from about 200 °C to 620 °C is assigned to the breakdown of the –COOH group in GO. These oxygen-functional groups make GO more hydrophilic compared to graphite, as a result a significant amount of water molecules is incorporated into the stacked structure of GO. Compared to the behavior of GO, the 3-chloropropyl-, 3-aminopropyl- and [Mn(TPyP)OAc]$^+Cl^-$-modified GO sheets exhibit different weight loss curves. When the temperature is less than 300 °C, only a slight weight loss is observed, probably still due to the thermal degradation of the unreacted oxygen functional groups of GO. The evident weight loss occurs in the range from 210 to 400 °C, which might be caused by the degradation of 3-chloropropyl and 3-aminopropyl chains attached onto the GO surface (see Supplementary Information). The reduction of weight loss at low temperatures results from the changes in the surface properties of GO by the replacement of its oxygen functional groups with $–NH_2$, –tart, and –Mn(porph) units. For $GO(NH_2)$ and GO-tart (= GO*) only a slight weigh loss of 10% occurs up 450 °C. Even up to 900 °C the two intermediates lose only about 20%. The material GO^*-$[Mn(TPyP)OAc]^+Cl^-$ that possesses all of the aforementioned attached groups shows a higher temperature

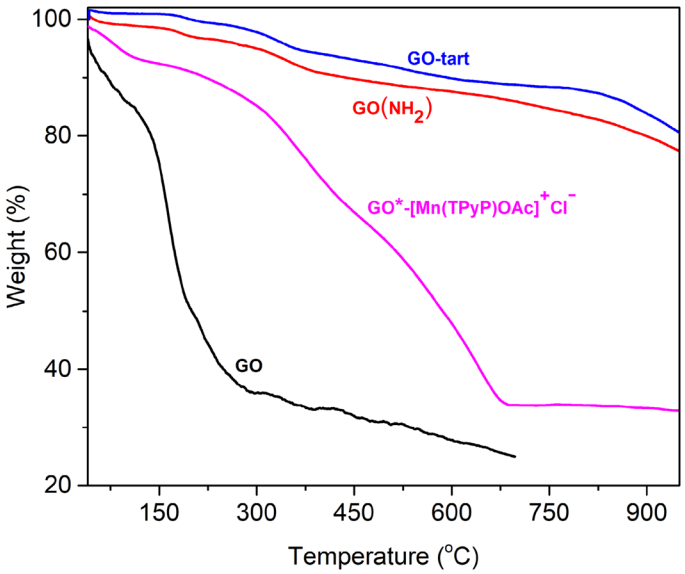

Fig. 3 Thermogravimetric (TGA) and DTG curves of $GO(NH_2)$, GO-tart and GO^*-$[Mn(TPyP)OAc]^+Cl^-$

for the maximum weight loss. For GO^*-[Mn(TPyP)tart], the mass loss before 100 °C is evidently related to the adsorbed water. The significant degradation step (28%) at 100 to 460 °C is related to decomposition of labile oxygen functionalities and the tartrate. The major weight loss of 32% at the temperatures ranging from 460 to 700 °C is attributed to the decomposition of Mn-porphyrin due to stability of the porphyrin ring up to higher than 600 °C [37].

3.5 SEM and TEM Studies

The morphology and microstructure of the GO sheets were assessed by scanning electron microscopy, SEM. The images of GO, GO^*-$[Mn(TPyP)OAc]^+Cl^-$ and used GO^*-$[Mn(TPyP)OAc]^+Cl^-$ after the fourth recycling are shown in Fig. 4. In Fig. 4a the typical wrinkling is clearly seen in the nanosheets of GO. During the catalyst preparation, GO preserves its wrinkled sheet texture without any transformation (Figs. 4b, 5). Some changes in the morphology of the catalyst GO^*-$[Mn(TPyP)OAc]^+Cl^-$ with respect to that of GO result from the increase of the steric hindrance by the covalent linkage of the porphyrin onto GO [38]. The TEM images reveal the well-distributed and separated $[Mn(TPyP)OAc]^+Cl^-$ species. The agglomeration on the planes of GO^*-$[Mn(TPyP)OAc]^+Cl^-$ is seen after five times use and recovering in the oxidation reaction of styrene (Fig. 4c).

3.6 Catalyst Activity

Styrene as a representative prochiral olefin was used for evaluation of the catalytic activity of GO^*-$[Mn(TPyP)OAc]^+Cl^-$. The optimization of the relevant parameters, namely temperature (20, 40 and 60 °C), solvent (CH_3CN, *n*-hexane, ethyl acetate) and reaction time (2 h, 4 h, 6 h) was achieved using the Box-Behnken method [39]. Maximum conversion and selectivity were obtained when the reaction was carried out in CH_3CN at 52 °C for 6 h. The homogeneous catalyst [Mn(TPyP)OAc] was more active than GO^*-$[Mn(TPyP)OAc]^+Cl^-$ and could catalyze the oxidation of styrene to styrene oxide in 4 h under the similar reaction conditions. However, the product was not asymmetric and the homogeneous catalyst could not be separated easily from the reaction mixture.

Various aromatic olefins and terminal linear olefins were successfully oxygenated under these optimized conditions with high enantioselectivity in the presence of GO^*-$[Mn(TPyP)OAc]^+Cl^-$. Activity and selectivity of the catalyst were substrate dependent. Styrene, α-methyl styrene and *trans*-stilbene were completely converted to the corresponding epoxide with enantioselectivities of more than 94% (Table 2, GC-chromatogram in the Supplementary Information). Presence of the benzylic positions improve the activity of styrene derivatives. It is interesting to note that even linear terminal olefins such as 1-octene (conversion 76%) and 1-decene (conversion 54%) were oxidized with enantiomeric excess values of 92% and 93%, respectively. In agreement with reported studies [32], the activity of terminal linear olefins was lower than those of the activated styrene derivatives (Table 2). Linear terminal olefins are electron deficient compounds with a long alkyl chain which could be the reason for their lower activity. These findings suggest the importance of a steric hindrance effect during the oxygen transfer from the active intermediate to the olefin. The limited conversion of terminal olefins has also been reported in the oxidation catalyzed by peroxygenases [40] and P450 models [41]. The lower conversion of terminal olefins is attributed to

(a) GO

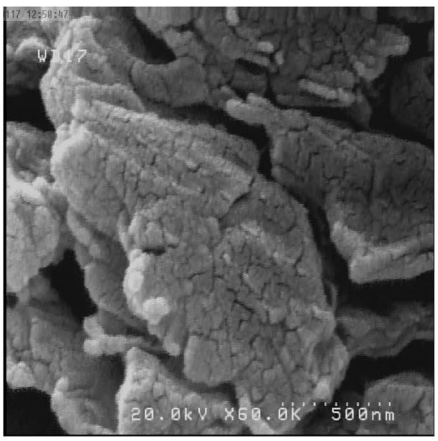

(a) GO

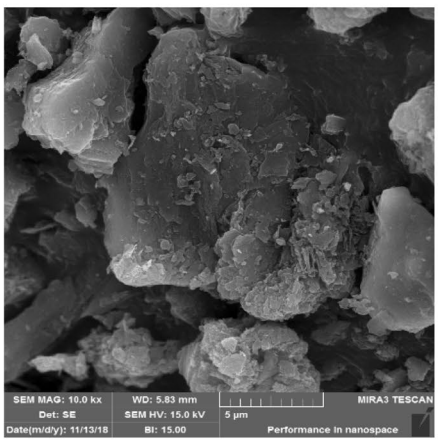

(b) GO*-[Mn(TPyP)OAc]$^{+}$Cl^{-}

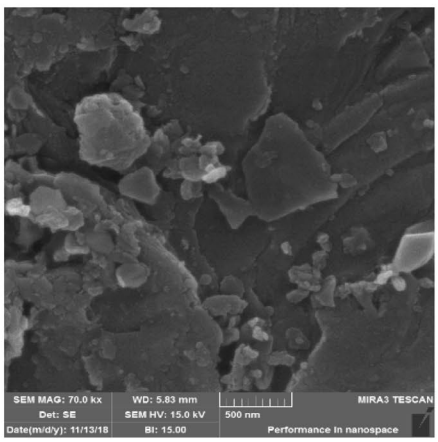

(b) GO*-[Mn(TPyP)OAc]$^{+}$Cl^{-}

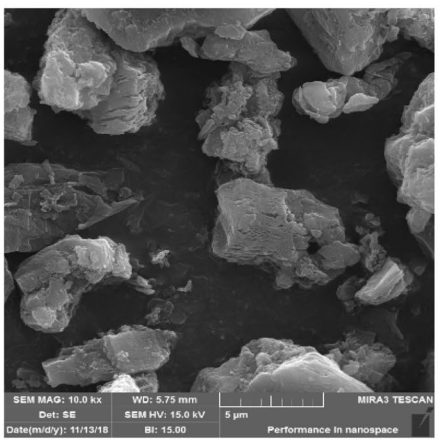

(c) GO*-[Mn(TPyP)OAc]$^{+}$Cl^{-} after fourth recycling

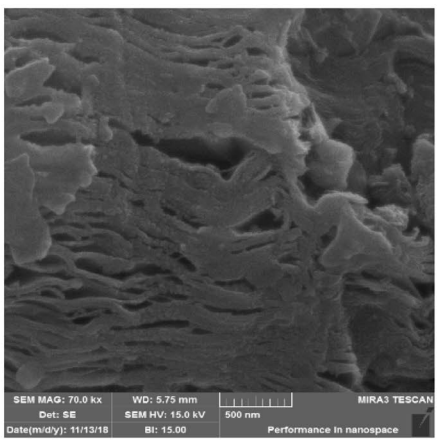

(c) GO*-[Mn(TPyP)OAc]$^{+}$Cl^{-} after fourth recycling

Fig. 4 SEM images of GO (**a**), fresh catalyst GO*-[Mn(TPyP)OAc]$^{+}$Cl^{-} (**b**) and used catalyst after fourth recycling (**c**) at different magnifications

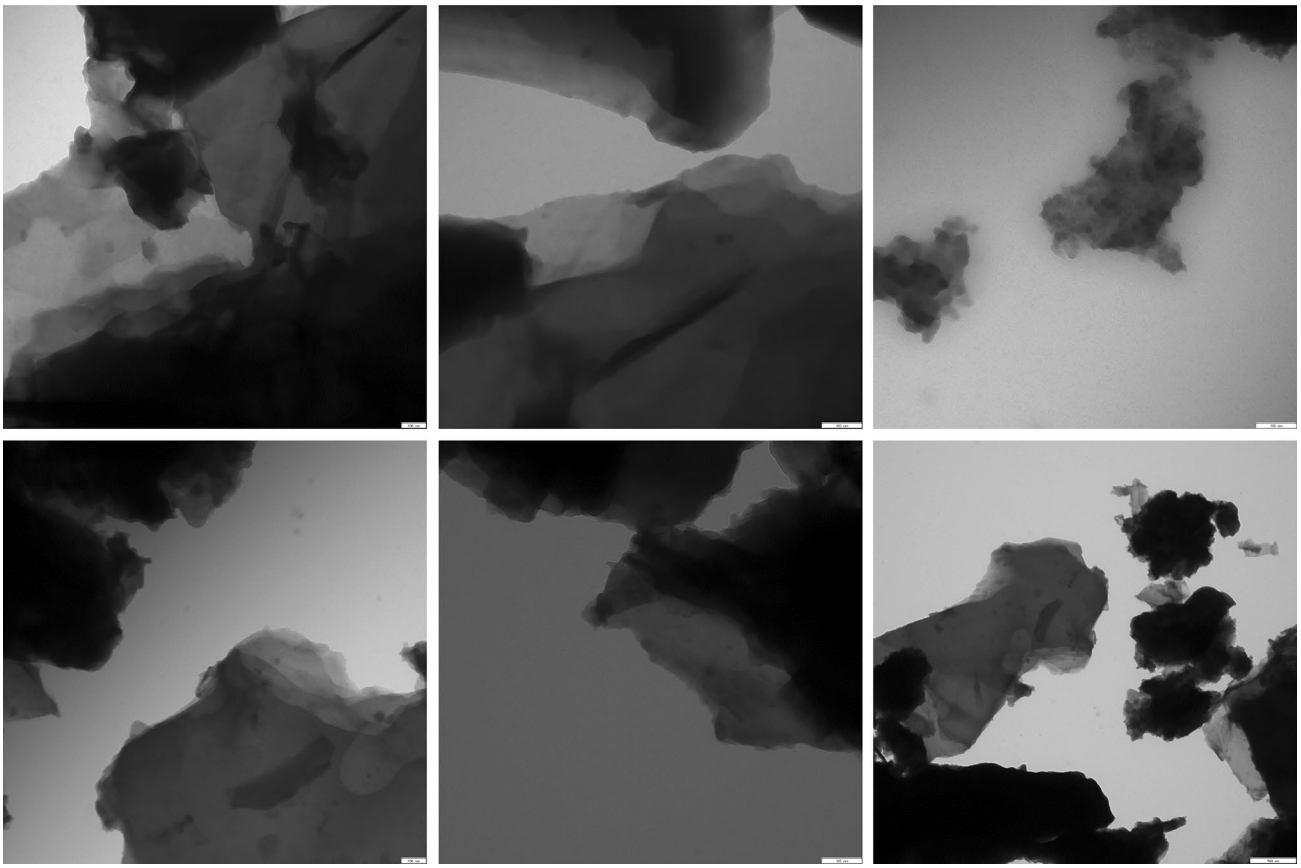

Fig. 5 TEM images of GO(NH_2)-[Mn(TPyP)OAc]$^+Cl^-$ (above) and GO*-[Mn(TPyP)OAc]$^+Cl^-$ (bottom). The scale bar is 100 nm for left and middle figures and 500 nm for the two right figures

Table 2 Enantioselective epoxidation of prochiral olefins

Entry	Substrate	Conv. (%)	ee (%) (Conf.)
1	Styrene	100	99 (*R*)
2	α-Methylstyrene	100	94 (*R*)
3	*trans*-Stilbene	100	100 (*R*,*R*)
4	1-octene	76	92 (*R*)
5	1-decene	54	93 (*R*)

Reaction conditions: catalyst GO*-[Mn(TPyP)OAc]$^+Cl^-$ 1.0 mg, olefin 1.0 mmol, oxygen balloon, isobutyraldehyde 3.0 mmol, CH_3CN 3 mL, temperature 52 °C, time 6 h

the heme alkylation by 1-alkenes that leads to the inactivation of the enzyme.

The high enantioselectivity of GO*-[Mn(TPyP)OAc]$^+Cl^-$ is much better than that of the catalyst GO-[Mn(TPyP)OAc]$^+$tart$^-$ (ee 73% for styrene and ee 58% for α-methyl styrene and *trans*-stilbene) where chirality is induced by a chiral, enantiopure L-tartrate (tart) counter ion [10]. These findings indicate the superior potential of the covalently bound tartrate onto GO in inducing chirality onto the catalytically active manganese-porphyrin unit.

To examine the recyclability of the catalyst, styrene (1.0 mmol), isobutyraldehyde (3.0 mmol) and the catalyst (1.0 mg) were added to CH_3CN (3.0 mL) and the reaction was followed under 1 atm of oxygen at 52 °C for 6 h by GC analysis. At the end, the heterogeneous catalyst was separated from the reaction mixture by centrifugation. The composition of the supernatant solution was studied by GC analysis. The remaining solid catalyst was washed with acetonitrile and centrifuged, then used for the next run after addition of styrene (1.0 mmol), isobutyraldehyde (3.0 mmol) and CH_3CN (3.0 mL). The conversion remained at almost 100% for the first four runs, and started only to decrease in the 5th run (Fig. 6). A reduction of 4% in styrene conversion was observed after five times recovery and reuse of the catalyst. This decrease in the activity of catalyst is partially due to its loss during recovery by sequential centrifugation and washing. In addition, reduction of conversion to 95.7% in the fourth run probably is due to agglomeration of the planes of GO*-[Mn(TPyP)OAc]$^+Cl^-$ (see Fig. 4c). After each recycle experiment, the possibility of leaching

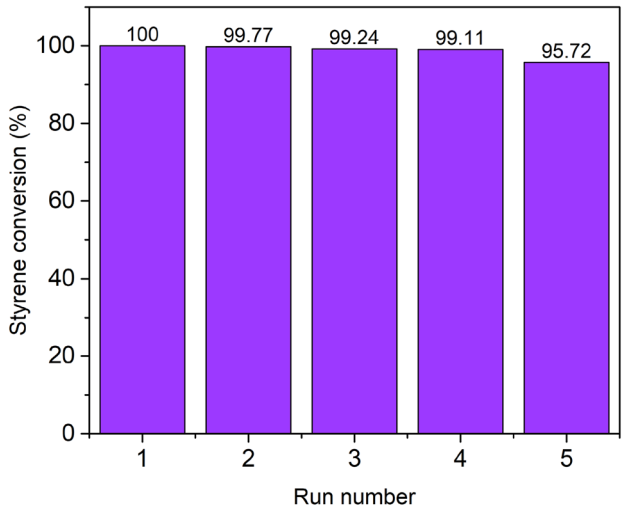

Fig. 6 The reusability of GO*-[Mn(TPyP)OAc]$^{+}$Cl^{-} in the oxidation of styrene with oxygen

manganese or porphyrine were investigated by analyzing the filtrate using atomic absorption spectroscopy (AAS) at wavelength 279.5 nm and UV–Vis spectroscopy in the range 200–800 nm, respectively. No traces of manganese (< 0.02 ppm), Mn-porphyrin or free porphyrin were detected.

3.7 Plausible Mechanism for the Epoxidation with ^{i}PrCHO/O_2 Catalyzed by GO*-[Mn(TPyP)OAc]$^{+}$Cl^{-}

Many reports confirm the formation of catalytically active high-valent manganese(IV or V) oxo porphyrins in the Mn-porphyrin catalyzed oxygenation of organic substrates [42–44]. It is well-known that a free radical reaction results in the formation of manganese oxo porphyrins in the presence of molecular oxygen and aldehyde as co-reductant [45]. Based on the observed results (Table 2) and other reported studies [46], a plausible mechanism can be proposed as given in Scheme 2 for the asymmetric aerobic

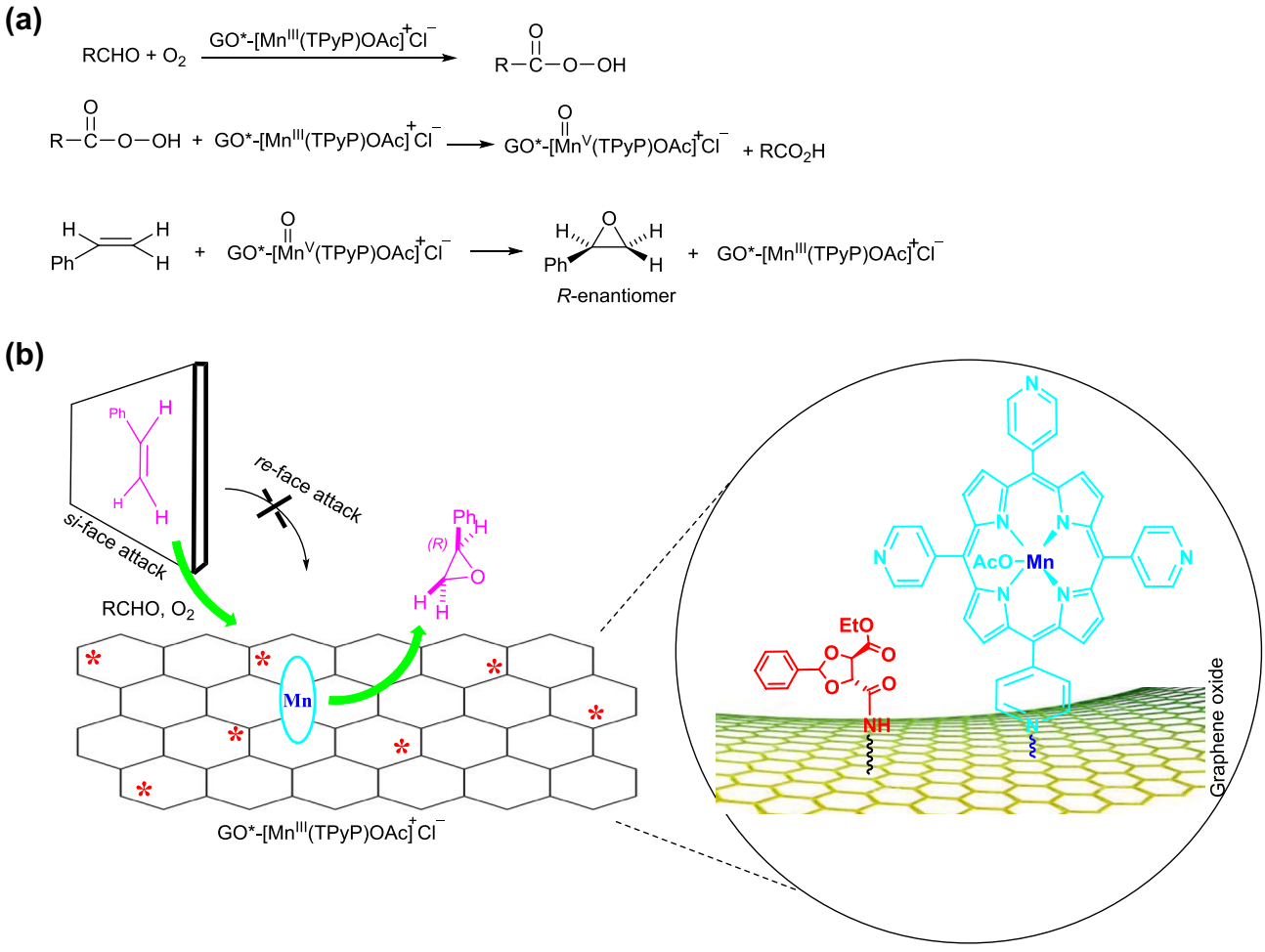

Scheme 2 Mechanism proposed for the asymmetric epoxidation of styrene (olefins) catalyzed by GO*-[Mn(TPyP)OAc]$^{+}$Cl^{-} using O_2 as the oxidant and isobutyraldehyde as a co-reductant

epoxidation of styrene as a representative olefin in the presence of GO*-[Mn(TPyP)OAc]$^{+}$Cl^{-} and isobutyraldehyde. First a peracid (RCO_3H) is formed by the treatment of O_2 and isobutyraldeyde (RCHO) which is catalyzed by the Mn-porphyrin via the involvement of an acyl peroxy radical (Scheme 2a). The subsequent reaction between the acyl peroxy acid and the Mn-porphyrin produces a catalytically active high-valent manganese oxo species, either a Mn(IV) oxo or Mn(V) oxo complex, which can readily oxidize an olefin to an epoxide while it is being reduced itself to a manganese(III) complex. This process is repeated many times before decomposition of manganese oxo species to μ-oxo dimeric manganese porphyrin or other catalytically inactive species [47]. Enantioselectivity of the catalyst GO*-[Mn(TPyP)OAc]$^{+}$Cl^{-} probably originates from enantioselective adsorption via non-covalent interaction of the prochiral olefin (styrene) with the chiral GO surface (GO*) which facilitates the oxygen atom transfer from the Mn = O intermediate to the si-face of the olefin; so that an enantiopure epoxide as the (*R*)-enantiomer resulted. The observed enantioselectivity can be rationalized by the nucleophilic attack of the olefin to the active intermediate Mn-oxo on the surface. The configuration of the epoxides indicates that the favorite face of the approaching carbon–carbon double bond to the Mn=O should be the pro-Si face. Chirality of GO* plays an active role in this preference face of the olefin by noncovalent interaction with the olefin (Scheme 2b).

There is no direct experimental evidence to show how close L-tartrate to the Mn-porphyrin is. However, indirect results of the catalytic epoxidation experiments (with ee 92–99%) suggest that the chiral inducer (L-tartrate ester) must be distributed evenly on the surface of GO and must be located close enough to the Mn-porphyrin to apply its chiral induction effect and to induce the approach of the prochiral olefin mainly via its pro-si face with high preference. Using this chiral-surface method can be an analogue to supramolecular strategies that are used to control activity and selectivity in hydroformylation reactions olefins [48].

4 Conclusion

To overcome the complicated issue of preparing active asymmetric catalyst, a chiral catalyst could be prepared by immobilizing the active catalyst on an asymmetric support. In this study a new chiral catalyst was successfully synthesized by grafting [Mn(TPyP)OAc] onto modified graphite oxide (GO) with a chiral L-tartrate ester to yield GO*-[Mn(TPyP)OAc]$^{+}$Cl^{-}. The immobilization of complex [Mn(TPyP)OAc]$^{+}$Cl^{-} onto GO and functionalization of GO are achieved uniformly. It was shown that this material is an efficient and enantioselective recyclable catalyst for the asymmetric oxygenation of olefins with oxygen/isobutyraldehyde under mild reaction conditions. Non-covalent interactions between GO* and the olefin facilitate the adsorption and interaction of the prochiral olefin preferentially through its si-face with the probable reactive intermediate [O=Mn^{V}(porphyrin)] which then leads to the enantiopure epoxide.

Acknowledgements The University of Zanjan is acknowledged for financial support. We thank the Center for Advanced Imaging (CAi) and Sophia Köhler of the Institut für Kolloide und Nanooptik of the Heinrich-Heine-Universität Düsseldorf for their support in obtaining the TEM images.

References

1. Crassous J (2009) Chiral transfer in coordination complexes: towards molecular materials. Chem Soc Rev 38:830–845
2. Chen J, Zhang T, Liu X, Shen L (2019) Enantioselective synthesis of (S)-γ-amino alcohols by Ru/Rh/Ir catalyzed asymmetric transfer hydrogenation (ATH) with tunable chiral tetraaza ligands in water. Catal Lett 149:601–609
3. Zhang X, Yin J, Yoon J (2014) Recent advances in development of chiral fluorescent and colorimetric sensors. Chem Rev 114:4918–4959
4. Luanphaisarnnont T, Hanprasit S, Somjit V, Ervithayasuporn V (2018) Chiral pyrrolidine bridged polyhedral oligomeric silsesquioxanes as heterogeneous catalysts for asymmetric michael additions. Catal Lett 148:779–786
5. Ding K, Uozumi Y (eds) (2008) Handbook of asymmetric heterogeneous catalysis. Wiley, New Jersey
6. Jacobsen EN, Pfaltz A, Yamamoto H (eds) (2003) Comprehensive asymmetric catalysis: Supplement 1. Springer, New York
7. Pélisson CH, Denicourt-Nowicki A, Meriadec C, Greneche JM, Roucoux A (2015) Magnetically recoverable palladium (0) nanocomposite catalyst for hydrogenation reactions in water. ChemCatChem 7:309–315
8. Kragl U, Dwars T (2001) The development of new methods for the recycling of chiral gcatalysts. Trends Biotechnol 19:442–449
9. Berijani K, Hosseini-Monfared H (2018) Collaborative effect of Mn-porphyrin and mesoporous SBA-15 in the enantioselective epoxidation of olefins with oxygen. Inorg Chim Acta 471:113–120
10. Berijani K, Farokhi A, Hosseini-Monfared H, Janiak C (2018) Enhanced enantioselective oxidation of olefins catalyzed by Mn-porphyrin immobilized on graphite oxide. Tetrahedron 74:2202–2210
11. Song CE, Lim JS, Kim SC, Lee KJ, Chi DY (2000) Immobilisation of ketone catalyst: a method to prevent ketone catalyst from decomposing during dioxirane-mediated epoxidation of alkenes. Chem Commun 24:2415–2416
12. Trindade AF, Gois PM, Afonso CA (2009) Recyclable stereoselective catalysts. Chem Rev 109:418–514
13. Heitbaum M, Glorius F, Escher I (2006) Asymmetric heterogeneous catalysis. Angew Chem Int Ed Engl 45:4732–4762
14. Fraile JM, Garcia JI, Mayoral JA (2008) Noncovalent immobilization of enantioselective catalysts. Chem Rev 109:360–417
15. Kaushik M, Basu K, Benoit C, Cirtiu CM, Vali H, Moores A (2015) Cellulose nanocrystals as chiral inducers: enantioselective catalysis and transmission electron microscopy 3D characterization. J Am Chem Soc 137:6124–6127

16. Wen Y, Sheng T, Xue Z, Sun Z, Wang Y, Hu S, Huang Y, Li J, Wu X (2014) Homochiral layered coordination polymers from chiral N-carbamylglutamate and achiral flexible bis (pyridine) ligands: syntheses, crystal structures, and properties. Cryst Growth Des 14:6230–6238
17. Dementyev P, Peter M, Adamovsky S, Schauermann S (2015) Chirally-modified metal surfaces: energetics of interaction with chiral molecules. Phys Chem Chem Phys 17:22726–22735
18. Holland MC, Meemken F, Baiker A, Gilmour R (2015) Chiral imidazolidinone and proline-derived surface modifiers for the Pt-catalysed asymmetric hydrogenation of activated ketones. J Mol Catal A: Chem 396:335–345
19. Gellman AJ, Tysoe WT, Zaera F (2015) Surface chemistry for enantioselective catalysis. Catal Lett 145:220–232
20. Zahed B, Hosseini-Monfared H (2015) A comparative study of silver-graphite oxide nanocomposites as a recyclable catalyst for the aerobic oxidation of benzyl alcohol: support effect. Appl Surf Sci 328:536–547
21. Su C, Loh KP (2012) Carbocatalysts: graphite oxide and its derivatives. Acc Chem Res 46:2275–2285
22. Fan W, Gao W, Zhang C, Tjiu WW, Pan J, Liu T (2012) Hybridization of graphene sheets and carbon-coated Fe_3O_4 nanoparticles as a synergistic adsorbent of organic dyes. J Mater Chem 22:25108–25115
23. Monnier JR (2001) The direct epoxidation of higher olefins using molecular oxygen. Appl Catal A 221:73–91
24. Marcano DC, Kosynkin DV, Berlin JM, Sinitskii A, Sun Z, Slesarev A, Alemany LB, Lu W, Tour JM (2010) Improved synthesis of graphite oxide. ACS Nano 4:4806–4814
25. Bhanja P, Das SK, Patra AK, Bhaumik A (2016) Functionalized graphite oxide as an efficient adsorbent for CO_2 capture and support for heterogeneous catalysis. RSC Adv 6:72055–72068
26. Alavi S, Hosseini-Monfared H, Aleshkevych P (2014) A highly efficient, enantioselective and recyclable mesoporous silica-based Mn(II) catalyst for asymmetric oxidation of thioanisole. RSC Adv 4:48827–48835
27. Farokhi A, Monfared HH (2017) Highly efficient asymmetric epoxidation of olefins with a chiral manganese-porphyrin covalently bound to mesoporous SBA-15: support effect. J Catal 352:229–238
28. Dreyer DR, Park S, Bielawski CW, Ruoff RS (2010) The chemistry of graphite oxide. Chem Soc Rev 39:228–240
29. Williams G, Seger B, Kamat PV (2008) TiO_2-graphene nanocomposites. UV-assisted photocatalytic reduction of graphite oxide. ACS Nano 2:1487–1491
30. Khoshroo M, Hosseini-Monfared H (2017) Oxidation of sulfides with H_2O_2 catalyzed by impregnated graphite oxide with Co–Cu–Zn doped Fe_3O_4/Co_3O_4–MoO_3 nanocomposite in acetonitrile. J Inorg Organomet Polym Mater 27:165–175
31. Hosseini SM, Hosseini-Monfared H, Abbasi V (2017) Silver ferrite–graphene nanocomposite and its good photocatalytic performance in air and visible light for organic dye removal. App Organomet Chem 31:e3589
32. Abbasi V, Hosseini-Monfared H, Hosseini SM (2017) Mn(III)-salan/graphite oxide/magnetite nanocomposite as a highly selective catalyst for aerobic epoxidation of olefins. Appl Organomet Chem 31:e3554
33. Kim KH, Yang M, Cho KM, Jun YS, Lee SB, Jung HT (2013) High quality reduced graphene oxide through repairing with multi-layered graphene ball nanostructures. Sci Rep 3:3251
34. Acik M, Lee G, Mattevi C, Chhowalla M, Cho K, Chabal YJ (2010) Unusual infrared-absorption mechanism in thermally reduced graphite oxide. Nat Mater 9:840–845
35. Fodor MA, Horváth O, Fodor L, Grampp G, Wankmüller A (2014) Photophysical and photocatalytic behavior of cobalt(III) 5,10,15,20-tetrakis(1-methylpyridinium-4-yl)porphyrin. Inorg Chem Commun 50:110–112
36. Valicsek Z, Horváth O (2013) Application of the electronic spectra of porphyrins for analytical purposes: the effects of metal ions and structural distortions. Microchem J 107:47–62
37. Lee KY, Lee YS, Kim S, Ha HM, Bae SE, Huh S, Jang HG, Lee SJ (2013) Morphological diversity of Mn(III) metalloporphyrin-based nano-and microsized CPAs assembled via kinetic and thermodynamic controls and their application in heterogeneous catalysis. CrystEngComm 15:9360–9363
38. Chen L, Guo X, Guo B, Cheng S, Wang F (2016) Electrochemical investigation of a metalloporphyrin–graphene composite modified electrode and its electrocatalysis on ascorbic Acid. J Electroanal Chem 760:105–112
39. Kabuk HA, İlhan F, Avsar Y, Kurt U, Apaydin O, Gonullu MT (2014) Investigation of leachate treatment with electrocoagulation and optimization by response surface methodology. Clean 42:571–577
40. Peter S, Kinne M, Ullrich R, Kayser G, Hofrichter M (2013) Epoxidation of linear, branched and cyclic alkenes catalyzed by unspecific peroxygenase. Enzyme Microb Technol 52:370–376
41. Collman JP, Hampton PD, Brauman JT (1990) Suicide inactivation of cytochrome P-450 model compounds by terminal olefins. 1. A mechanistic study of heme N-alkylation and epoxidation. J Am Chem Soc 112:2977–2986
42. Groves JT, Lee J, Marla SS (1997) Detection and characterization of an oxomanganese(V) porphyrin complex by rapid-mixing stopped-flow spectrophotometry. J Am Chem Soc 119:6269–6273
43. Monnereau C, Ramos PH, Deutman ABC, Elemans JAAW, Nolte RJM, Rowan AE (2010) Porphyrin macrocyclic catalysts for the processive oxidation of polymer substrates. J Am Chem Soc 132:1529–1531
44. Den Boer D, Li M, Habets T, Iavicoli P, Rowan AE, Nolte RJM, Elemans JA (2013) Detection of different oxidation states of individual manganese porphyrins during their reaction with oxygen at a solid/liquid interface. Nat Chem 5:621–627
45. Nam W, Kim HJ, Kim SH, Ho RYN, Valentine JS (1996) Metal complex-catalyzed epoxidation of olefins by dioxygen with co-oxidation of aldehydes. A mechanistic study. Inorg Chem 35:1045–1049
46. Zhou X, Ji H (2010) Biomimetic kinetics and mechanism of cyclohexene epoxidation catalyzed by metalloporphyrins. Chem Eng J 156:411–417
47. Smegal JA, Schardt BC, Hill CL (1983) Isolation, purification, and characterization of intermediate (iodosylbenzene)metalloporphyrin complexes from the (tetraphenylporphinato)manganese(III)-Iodosyl-benzene catalytic hydrocarbon functionalization system. J Am Chem Soc 105:3510–3515
48. Nurttila SS, Linnebank PR, Krachko T, Reek JN (2018) Supramolecular approaches to control activity and selectivity in hydroformylation catalysis. ACS Catal 8:3469–3488

Affiliations

Elahe Ahadi[1] · Hassan Hosseini-Monfared[1,2] · Carsten Schlüsener[3] · Christoph Janiak[3] · Afsaneh Farokhi[1]

Christoph Janiak
janiak@hhu.de

[1] Department of Chemistry, University of Zanjan, Zanjan 45195-313, Iran

[2] Department of Chemistry, Amirkabir University of Technology, Tehran, Iran

[3] Institut für Anorganische Chemie und Strukturchemie, Heinrich-Heine-Universität, 40204 Düsseldorf, Germany